LASER VIBROMETRY BASED PRECISE MEASUREMENT OF TAPE-SHAPED TETHERS DAMPING RATIO TOWARDS SPACE APPLICATIONS

Andrea Valmorbida, Alice Brunello, Lorenzo Olivieri, Simone Fortuna, Giulia Sarego,
Marco Pertile and Enrico C. Lorenzini

Abstract—To mitigate the growing problem of space debris, current international guidelines require spacecraft in Low Earth Orbit (LEO) to implement post-mission disposal strategies to be deorbited within 25 years from the end of their operative life. Electrodynamic tethers are an effective and promising option for deorbiting as they do not require fuel consumption. However, the success of this new technology also depends on the dynamic stability of thin tape-shaped tethers during both deployment and deorbiting phases. This is where precise measurement of damping characteristics of thin tape-shaped tethers comes in.

This paper presents an innovative experimental setup and analysis methods for precisely measuring the damping ratio of a thin (thickness 50 microns) tape-shaped tether made of PEEK intended for use in electrodynamic tethers applications. To capture longitudinal oscillations during dynamic tests, we employed a laser vibrometer and explored four different methods of experimental data analysis, comparing and describing them in detail in the paper. We also conducted an uncertainty analysis in line with ISO GUM. The experimental results show good agreement among the four methods used to estimate the damping ratio with the most precise method involving nonlinear regression applied to all the experimental data. A Monte Carlo analysis was carried out considering the most significant sources of uncertainty. The smallest uncertainty interval is ±1% of the estimated damping ratio, with a 95% confidence level, using this method.

Index Terms— mechanical characteristics measurement, damping ratio estimation, laser vibrometer, thin tape-shaped tethers for space applications

I. INTRODUCTION

Since the beginning of the space era, the number of artificial satellites orbiting the Earth has continuously grown [1], mostly in Low Earth Orbits (LEO)[1], where they are utilized for scientific and commercial missions such as the mega-constellations OneWeb or Starlink by SpaceX [2]. However, only 6% of objects in orbit are operative [1], with the rest being inoperative satellites or fragments called space debris [3] that pose a real danger to operative satellites. The need to mitigate the growth of orbital debris is increasingly evident [4][5][6], and responsible conduct and self-regulation are being advocated by the space community [7][8][9]. It is strongly recommended that spacecraft in LEO are made to re-enter the atmosphere within 25 years of the end of their operational life (see guideline 6 of [10], [11] and [12]).

Green deorbiting technologies and strategies alternative to traditional chemical propulsion are under investigation [13][14] and Electrodynamic Tethers (EDTs) are considered a promising option [15][16][17] for their minimal impact on the space environment [18], due to the fact that they can generate thrust or drag forces without using propellant. Tape-shaped tethers have been studied in detail for their greater mass efficiency in collecting electrons from the Earth ionosphere [19] to produces the Lorentz force and higher survivability against space debris impacts compared to round tethers [20][21][22][23]. A thin tape-shaped tether with the same mass of a round tether has a larger external surface area for collecting ionospheric electrons [19] and is less likely to be completely severed by small debris impacts [21][23].

In this context, the team of the H2020 Future Emerging Technologies FET-OPEN project E.T.PACK[2,3], of which the University of Padova is a partner, has developed and built a Deorbit Kit prototype based on electrodynamic tether technology using a tape-shaped tether with two segments in series made of different materials [24]. The determination of tape tethers elastic and damping characteristics is important because those properties affect the dynamic response during deployment and the system stability during deorbiting [25]. Among the materials that can be used for tethers, PEEK (polyether ether ketone) is an appealing material because of its excellent mechanical and chemical resistance properties [26]. A hundred-meter portion of a thin (50 μm thickness) tape-shaped tether made of PEEK is used as a dynamic stabilizer for E.T.PACK [27][28] involving two benefits as follows. Firstly, it

A. Valmorbida is with the Dept. of Industrial Engineering (DII) of the University of Padova, Italy. (e-mail: andrea.valmorbida@unipd.it).

A. Brunello is with the Center of Studies and Activities for Space "G. Colombo" (CISAS), University of Padova, Italy. (e-mail: alice.brunello.3@phd.unipd.it).

L. Olivieri is with the Center of Studies and Activities for Space "G. Colombo" (CISAS), University of Padova, Italy. (e-mail: lorenzo.olivieri@unipd.it).

S. Fortuna is with the Center of Studies and Activities for Space "G. Colombo" (CISAS), University of Padova, Italy. (e-mail: simone.fortuna@phd.unipd.it).

G. Sarego was with the Center of Studies and Activities for Space "G. Colombo" (CISAS), University of Padova, Italy. (e-mail: giulia.sarego@unipd.it).

M. Pertile is with the Dept. of Industrial Engineering (DII) of the University of Padova, Italy. (e-mail: marco.pertile@unipd.it).

E. C. Lorenzini is with the Dept. of Industrial Engineering (DII) of the University of Padova, Italy. (e-mail: enrico.lorenzini@unipd.it).

[1] Orbital altitudes between 200 km and 2000 km.
[2] https://etpack.eu/
[3] https://aerospaceamerica.aiaa.org/year-in-review/space-tethers-focus-on-deorbit-and-debris-mitigation/

This article has been accepted for publication in IEEE Transactions on Instrumentation and Measurement. This is the author's version which has not been fully edited and

2

increases the total length of the tether: the higher the tether total length, the more stable the tethered system [20]; secondly, it contributes to the damping of the tape longitudinal oscillations and eventually to bounding the system librational dynamics that could cause the tethered system to flip upside-down (i.e., a tethered system instability) [24].

Material properties can be measured through various methods, which may lead to inconsistent data, especially for damping ratio values [29]. Due to their shape, thin tape-shaped tethers present a small bending and torsional rigidity and, for this type of measurement, are usually hanged vertically by clamping the upper end and tensioned by adding a weight to the lower end [30][22]. For vertical setups, particular care shall be given to the suspension structure, whose stiffness and damping shall be well separated from the parameters of the tape sample [29]. Mechanical parameters are reconstructed from static and dynamic measurements; in the latter case, laser vibrometers [31] or piezometric transducers [32] are employed. Once displacement data is collected, the Young's modulus calculation is straightforward; on the contrary, different methods can be employed to derive the damping ratio [32]. Low-friction testing facilities, as the one described in [33], can also be employed to estimate the elastic modulus and the damping coefficient of tape-shaped and round tethers for space applications [34] but requiring a more complex setup.

This paper, which is an extension of the proceedings paper [35], describes the use of a laser vibrometer to measure precisely the damping ratio of a thin (i.e., a thickness of 50 μm) tape-shaped tether made of PEEK used for space tether applications. The outline of this article is as follows. Section II introduces the proposed approach, providing a comparison with other approaches for damping properties measurement. Section III introduces the experimental setup and the measurement systems employed in this work. Section IV presents the data analysis methodology, describing four methods used for calculating the damping ratio, and introduces the uncertainty analysis. Lastly, the experimental results are shown and commented in Section V, followed by the final remarks in Section VI.

This paper adds new and substantial contributions to Ref. [35]. It provides additional context and references related to the topic in section I, introduces the proposed approach and compares it with other approaches in section II. Section III presents further technical and metrological details, an additional method of data analysis of the experimental data, and computation of error risk from Monte Carlo simulations. In section V, the new method's results are compared with other methods, and uncertainty intervals for the four analysis methods are computed and compared. As a general contribution, this paper provides a detailed and thorough uncertainty evaluation according to the ISO guide for a complex case important for future space applications, which serves as an example applicable to other cases and applications, considering relevant uncertainty sources and their analysis.

The novel contributions of this work relies in different elements combined together: 1) the use of a laser vibrometer to measure without contact the damping properties of a thin tape-shaped tether as a valid alternative to a traditional approach based on traction machines; 2) the experimental setup employed to induce and capture the longitudinal vibrations of the tape; 3)

a comparison between 4 methods to analyze the experimental data; and 4) a meticulous uncertainty analysis carried out according to standards (ISO-GUM) in order to properly compare the results of the 4 analysis methods. All these elements bring to a precise measurement of thin tape-shaped tethers damping ratio with an uncertainty interval of ±1% of the estimated damping ratio with a confidence level of 95%.

II. PROPOSED APPROACH

We present an experimental setup based on laser vibrometry and analysis methods of the experimental data to measure precisely the damping properties of thin (tens of microns) tape-shaped tethers that are used for space tethered systems. Specifically, the tape made of PEEK employed for the E.T.PACK project has a cross section of 50 μm x 25 mm; in addition, PEEK has a maximum yield stress of 120 MPa[4].

The authors of [36] developed a system to measure the structural damping coefficients of test samples with a cylindrical shape (10 mm in diameter and 100 mm in length) and made of different types of glasses. An automatically-actuated hammer is used to induce flexural dynamics on the cylindrical sample and two measurement systems are employed and compared to measure its vibration: a laser doppler vibrometer and a microphone. Analyzing laser vibrometer data, the damping ration was estimated by the experimenters with an uncertainty in the range ±6% - ±18% at 2σ confidence level, depending on the glass type. The experimental setup proposed in [36] can not be applied to measure the damping properties of a thin tape.

Another approach to measure the damping properties of materials consists in employing a traction machine to produce a cyclic force profile to a test sample (usually with a dumbbell shape) and measures the corresponding cyclic elongation profile [37][38]. The damping coefficient C of the test sample is estimated by evaluating the areas of the hysteresis cycles on the force-elongation graph according to the following equation:

$$C = \frac{\alpha}{\Omega \, \pi \, |X_p|^2} \qquad (1)$$

where α is the area of one hysteresis cycle in the force-elongation graph, Ω is the frequency of the cyclic force profile and X_p is the amplitude of the resulting cyclic elongation profile. Using this approach, the damping coefficient is estimated based on three quantities evaluated from the force and elongation profiles of the samples. When testing tape-shaped tethers with a thickness of tens of microns, there are two problems related to this approach. Firstly, the yield force of a thin tape is much lower than the yield force of a thicker dumbbell-shaped sample made of the same material and the test would require a pull machine that operates with a very fine resolution at a dynamic range that is about 1% of the usual pull machines operating at tens of kN. Secondly, the amount of material that absorbs the energy during the hysteresis cycles is small for a thin tape when compared to a thicker dumbbell-shaped sample. As a consequence, the resulting areas of the hysteresis cycles are very small, the impact of measurements noise on both the applied force and the resulting elongation is high, and the estimation of the damping factor is poor.

In contrast, the proposed approach estimates the damping ratio by accurately measuring without contact the longitudinal

---

This article has been accepted for publication in IEEE Transactions on Instrumentation and Measurement. This is the author's version which has not been fully edited and

3

free oscillations of longer samples of tape using a laser vibrometer with a 1 µm resolution (see later on). It has fewer sources of uncertainty when compared to the pull machine approach, leading to an overall reduced uncertainty. Additionally, apart from the laser vibrometer and the acquisition system that can be used for many other applications, the experimental setup consists of simple and low-cost mechanical and electrical components, as described in detail in Section III.

Although the proposed measurement method is applied to a tape-shaped tether made of PEEK used in space applications, it can also be applied to tapes of different materials and for other applications where a precise measurement of the damping ratio is required. In addition, all the experimental tests shown in the paper were conducted at ambient temperature, i.e., 20 °C ± 1 °C, and the measured value of the damping ratio is valid for that temperature range. The damping properties of material can vary with temperature and a similar measurement apparatus can be used in a thermal-vacuum chamber in the temperature range expected for a specific application, but the chamber will need to be vertical and relatively large.

The estimation of the elastic modulus E of the tape-shaped tether made of PEEK is also required. To this aim, an analog probe indicator with resolution of $10\ \mu m$ was used to first record the elongation Δx_i of a portion of tether vs. the applied force F_i during static tests. A linear least-square regression analysis of the experimental points ($\Delta x_i, F_i$) was then employed to estimate the elastic constant of the system K and its standard uncertainty. The PEEK Young's modulus E was then calculated as $E = KL_0/A_{cs}$, where A_{cs} is the tether cross section area and L_0 is the sample length. A more detailed description of the experimental setup and the methodology of analysis for this application, including the uncertainty analysis, can be found in [35].
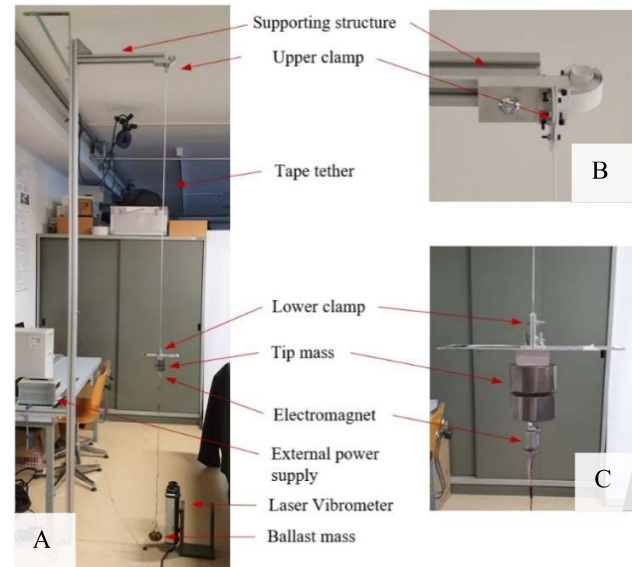
III. EXPERIMENTAL SETUP

Fig. 1 shows the experimental setup used to measure the damping ratio ζ of the tether during dynamic tests; a schematic representation of the same setup is depicted in Fig. 2. An external supporting structure blocks one end of the tape tether through an upper clamp (panel B of Fig. 1); the other tip of the tape tether is connected to a lower tip mass through a second clamp (panel C of Fig. 1). The external supporting structure is realized with Aluminum beam profiles and allows to change easily the tape tether length to be tested. In addition, a ballast mass is connected to the tip mass through a wire and an electromagnet energized by an external power supplier (panel C of Fig. 1). When the electromagnet is de-energized and the ballast mass is released, the tip mass starts oscillating and a laser vibrometer is used to measure the resulting oscillation.

Specifically, the laser vibrometer used is a heterodyne interferometer by Polytec composed of two modules: an optical module that emits a class II Helium Neon laser beam with a wavelength of $632.8\ nm$ and an electronic module that provides a velocity channel and a position channel as output. The sensitivity of the vibrometer was set at $25\ mm/s/V$ for the velocity channel and $1.28\ mm/V$ for the position channel. Both position and velocity channels were acquired at a frequency of 25 kHz employing the acquisition board National Instrument (NI 9215) through a NI Chassis CompactDAQ 9174 connected to the desktop PC of the laboratory. The acquisition board measures the input voltage in the range $\pm 10\ V$ using a 16-bit ADC. The resolution of the laser vibrometer for the position measurement is of the order of the laser wavelength, while the

resolution of the position measurement due to the acquisition system is $0.38\ \mu m$; therefore, the resolution of the measurement system composed of the laser vibrometer and the acquisition system is less than $1\ \mu m$.

All the experimental tests presented in this paper and concerning the damping ratio estimation were conducted with a tape of length $L_T = 1.5\ m$ and a tip mass with mass $m_{TM} = 1.627\ kg$. The tape tether cross-section area $A_{cs} = 25\ mm$ x $50\ \mu m = 1.25\ 10^{-6} m^2$.


Fig. 1. Experimental setup used for the damping ratio estimation of the tape tether (panel A), with details of the tether connections to the supporting structure (panel B) and to the tip mass with the electromagnet (panel C).
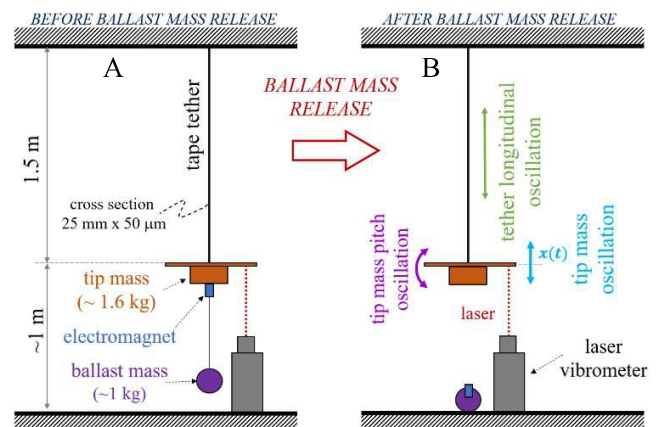
Fig. 2. Schematic representation of the experimental setup used for the damping ratio measurement (panel A) and effects of the ballast mass release (panel B). A laser vibrometer measures the displacement $x(t)$ of the tip mass after the release of the ballast mass.

IV. METHODOLOGY OF ANALYSIS

The measurement chain and data analysis steps followed for the determination of the tape tether damping ratio ζ are summarized in Fig. 3. The damping ratio estimation is based on dynamic tests and four types of analysis methods of the experimental data are considered and compared.
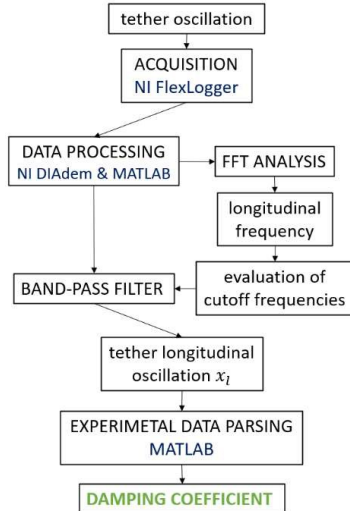
Fig. 3. Block diagram showing the measurement and data analysis chain for the determination of the tape tether damping coefficient. Additional details are provided as supplementary material of this paper.

B. Damping ratio estimation

Referring to Fig. 2, the laser vibrometer measures the displacement of the tip mass $x(t)$ after the release of the ballast mass. A frequency analysis of the signal $x(t)$ through a Fast Fourier Transform (FFT) of Matlab$^\copyright$ allowed us to first identify the component of $x(t)$ associated with the longitudinal oscillation of the tape, $x_l(t)$, and then to extract $x_l(t)$ by applying a band-pass filter to $x(t)$. The use of a band-pass filter is required because the tape and the tip mass experience not only an oscillation along the tape longitudinal axis, which is the vibrating mode of interest, but also other oscillations, mainly a pitch oscillation of the tip mass. The system was designed to reduce those oscillations as much as possible, but it was not possible to cancel them out completely. However, their frequencies are well separated from the longitudinal frequency and consequently they can be filtered out.
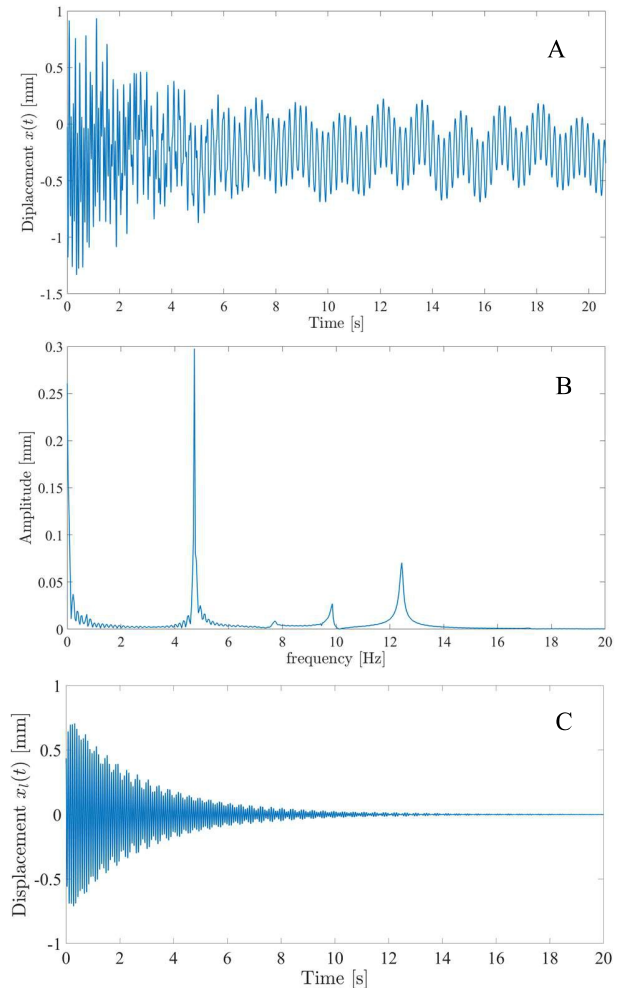
Fig. 4 shows the frequency spectrum, computed through the FFT, of a typical time profile of the tip mass displacement $x(t)$ measured by the laser vibrometer. The frequency spectrum of $x(t)$ reveals the presence of different peaks corresponding to the various vibrating modes of the system. Among them, the peak between $12\ Hz$ and $13\ Hz$ corresponds to the longitudinal oscillation of the tape and is of interest for the estimation of the damping ratio ζ of the tape tether. In addition, the peak between $4\ Hz$ and $5\ Hz$ corresponds to the pitch oscillation of the tip mass.

The system composed of the tape tether with the tip mass can be modelled as a mass-spring-damper system where the mass is almost completely that of the tip mass (the mass of the tether is about 1 gram and is negligible compared to the mass of the tip mass) and the spring and damper are associated with the

tape tether itself. The natural frequency of the longitudinal oscillation of the tape is:

$$f_n = \frac{1}{2\,\pi}\sqrt{\frac{E_{PEEK}\,A_{CS}}{L_T\,m_{TM}}} \approx (12.06 \pm 0.46)\ Hz \qquad (1)$$

where $E_{PEEK} = 3.74\ GPa$ is the Young's modulus of the PEEK estimated through static tests as described in [35].

Fig. 4. Typical time profile of the tip mass displacement $x(t)$ measured by the laser vibrometer (panel A), the corresponding frequency spectrum computed through FFT analysis (panel B), and the filtered signal (panel C).

Because the various peaks in the amplitude spectrum are well separated in frequency, it is possible to extract the longitudinal oscillation of the tape $x_l(t)$ from the total measured displacement of the tip mass $x(t)$ by filtering. Specifically, a low-pass Butterworth digital filter with a cutoff frequency of $400\ Hz$ was first applied to remove the high-frequency noise. After that, a high-pass elliptical filter with a cutoff frequency of $10.6\ Hz$ was employed to remove those oscillations associated with the tip mass pitch motion and the vibration of the supporting structure.

Using the filtered signal $x_l(t)$, four methods were employed for the computation of the damping ratio ζ, as described in the following. The tether with the tip mass attached to the free end is modelled as 1 Degree of Freedom (DOF) 2nd

This article has been accepted for publication in IEEE Transactions on Instrumentation and Measurement. This is the author's version which has not been fully edited and

5

order underdamped system ($\zeta < 1$) with an initial displacement with respect to the equilibrium position $x_{l,0}$ and null initial velocity $\dot{x}_{l,0}$.

Method 1: logarithmic decrement

Method 1 is based on the estimation of the rate with which the amplitude of the damped vibration $x_l(t)$ decreases. The damping ratio ζ is computed using the logarithmic decrement formula:

$$\zeta_r = \frac{-\ln\frac{g_r}{g_1}}{\sqrt{\left(\ln\frac{g_r}{g_1}\right)^2 + (r\,\pi)^2}} \qquad (2)$$

where g_1 id the amplitude of $x_l(t)$ at the first peak and g_r is the amplitude of $x_l(t)$ at the r-th peak or valley, where r is the peak or valley index (see also Fig. 5).

Method 2: linear regression on peaks and valleys envelope

Method 2 is based on a linear regression applied to the natural logarithm of peaks or valleys of the filtered signal $x_l(t)$. The extrema points, i.e., peaks or valleys, of $x_l(t)$ are computed as maximum or minimum values of $x_l(t)$, respectively. The resulting peaks and valleys are denoted as $(p_i, t_{p,i})$ and $(v_i, t_{v,i})$, respectively. Applying the natural logarithm to the envelope of the peaks of a 2nd order underdamped system ($\zeta < 1$), the following equations is obtained (see also Fig. 5):

$$y = A\,t + B \qquad (3)$$

where $y = \ln p$, $A = -\zeta\omega_n$ and $B = \ln a$. Furthermore, $\omega_n = \sqrt{k/m}$ is the natural frequency of the system, $k = EA/L$ is the tape elastic constant of the system and m is mass of the tip mass. A linear regression can be applied to the experimental values $(y_i, t_{p,i})$, with $y_i = \ln p_i$, in order to calculate the values of A and B that minimize the sum of the squared residuals $r_i = y_i - (A\,t_{p,i} + B)$. The value of ζ is then computed as $\zeta = -A/\omega_n$. A similar procedure can be applied to the valleys $(v_i, t_{v,i})$ of the signal $x_l(t)$.
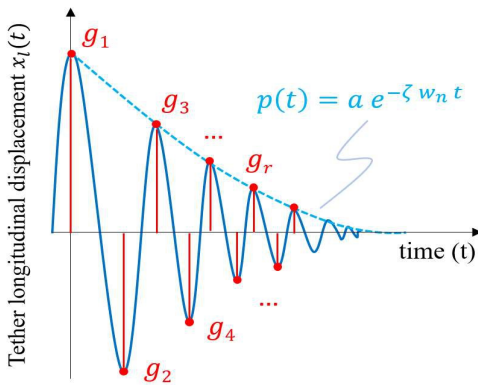
Fig. 5. Tether longitudinal displacement in continuous dark blue line with the envelope of the peaks in dashed light blue line and peaks and valleys marked by red dots used in methods 1, 2 and 3.

Method 3: nonlinear regression on peaks and valleys envelope

Method 3 is based on a nonlinear regression applied to peaks or valleys of the filtered signal $x_l(t)$. The extrema points, i.e.

peaks or valleys, of $x_l(t)$ are computed as maximum or minimum values of $x_l(t)$, respectively, and the resulting peaks and valleys are denoted as $(p_i, t_{p,i})$ and $(v_i, t_{v,i})$, respectively. For a 1 DOF 2nd-order underdamped system ($\zeta < 1$), the envelope of the peaks has the following expression:

$$p(t) = a\,e^{-\zeta\omega_n t} = a\,e^{bt} \qquad (4)$$

where $b = -\zeta\omega_n$ and the other parameters have been defined previously. The Matlab$^{©}$ optimization toolbox was used to compute the values of a and b that minimize the sum of the squared residuals $r_i = p_i - a\,e^{bt_i}$. The value of ζ is then computed as $\zeta = -b/\omega_n$, where A, L and m required for the computation of ω_n, are measured with a caliper, a ruler, and a balance, respectively. A similar procedure can be applied to the valleys $(v_i, t_{v,i})$ of the signal $x_l(t)$.

Method 4: nonlinear regression of filtered experimental data

Method 4 is based on a nonlinear regression applied to the complete data set of the signal $x_l(t)$. Indeed, the response of a 2nd-order underdamped system to initial displacement $x_{l,0}$ with respect to the equilibrium position and null initial velocity $\dot{x}_{l,0}$ can be written as:

$$x_l(t) = \sqrt{c_1^2 + c_2^2} \cdot e^{-\zeta\omega_n t} \cdot \cos(\omega_d t - \phi) \qquad (5)$$

Where $\omega_d = \omega_n\sqrt{1 - \zeta^2}$ is the observed natural frequency, $c_1 = x_{l,0}$, $c_2 = (\dot{x}_{l,0} + \zeta\omega_n x_{l,0})/\omega_d$ and $\phi = \text{atan}(c_2/c_1)$. The Matlab$^{©}$ optimization toolbox can be used to compute the values of x_0, $\dot{x}_{l,0}$, ω_n and ζ that minimize the sum of the squared residuals $r_i = x_i - x_l(t_i)$, where x_l is computed using (5).

C. UNCERTAINTY ANALYSIS

The uncertainty analysis was conducted according to GUM [39]. Two kinds of uncertainties were estimated. The first one is a repeatability extended uncertainty U_ζ computed for each method and due to the repetition of experimental tests in the same operative conditions. Specifically, U_ζ was computed as $U_\zeta = t_{1-\frac{\alpha}{2},N-1} \cdot u_\zeta$, where $t_{1-\frac{\alpha}{2},N-1}$ is the coverage factor computed from the t-Student distribution with an error risk of 5% and a number of degree of freedom $N - 1$, being N the number of tests performed, and u_ζ the standard uncertainty computed as standard deviation of the values of ζ obtained from the N experimental tests.

The second kind of uncertainty is the extended uncertainty $\widetilde{U}_\zeta$ associated with the outcome of each method and each acquisition and due to the uncertainty sources. In particular, three main uncertainty sources were considered: a) the displacement of the tip mass measured by the laser vibrometer; b) the cutoff frequencies of the pass-band filter; and c) the parameters used in each method, including the initialization values of the parameters involved in the optimization process for method 3. In other words, the uncertainty sources are due to the measurement system utilized and the methods of data analysis used to estimate the damping ratio ζ.

Considering that the mathematical model relating the quantity being estimated, i.e., ζ, and the input quantities that are considered the uncertainty sources is nonlinear, we performed a Monte Carlo (MC) analysis with a number of trials $M = 10000$ to evaluate $\widetilde{U}_\zeta$, following the Supplement 1 to the GUM [40]. Specifically, Table I lists the uncertainty sources

considered in the MC analysis, including the Probability Density Function (PDF) used to generate the M values of each uncertainty source and the parameters that define the PDF. For a uniform PDF, the parameter a indicates the width of the interval in which the uniform distribution is defined. The uncertainty source due to the measurement system resolution was not considered in the MC analysis because its contribution is one order of magnitude lower than the vibrometer accuracy.

TABLE I
UNCERTAINTY SOURCES USED IN THE MONTE CARLO ANALISYS FOR THE THREE METHODS

Uncertainty source	PDF	PDF parameter
Vibrometer accuracy[5]	Gaussian	$\sigma = 10\ \mu m$
Lower cutoff frequency, $f_{c,L}$	Uniform	$a_{f_{c,L}}/2 = 1\ Hz$
Higher cutoff frequency, $f_{c,L}$	Uniform	$a_{f_{c,H}}/2 = 100\ Hz$
Methods 1, 2 and 3		
tape elastic modulus E	Uniform	$a_E = 0.2\ GPa$
tape thickness t	Uniform	$a_t = 5\ \mu m$
tape width w	Uniform	$a_w = 0.05\ mm$
tape length L	Uniform	$a_L = 1\ mm$
tip-mass mass m	Uniform	$a_m = 1\ gram$
Method 4		
Initial ω_n	Uniform	$a_{\omega_n}/2 = 40\ rad/s$
Initial ζ	Uniform	$a_\zeta/2 = 4 \cdot 10^{-3}$
Initial $\dot{x}_{l,0}$	Uniform	$a_{\dot{x}_{l,0}}/2 = 0.5\ mm/s$

Preliminary MC analysis revealed that the PDF of the damping ratio ζ, evaluated as the frequency histogram using the 10000 values of ζ from the MC analysis, is in general not symmetric. Consequently, the coverage factor used for the computation of the extended uncertainty $\tilde{U}_\zeta$ was evaluated following the Supplement 1 to the GUM [40]. Specifically, the following definitions are given: p is the probability associated with the confidence level, α is half of the error risk and G_ζ is an approximation (obtained from the histogram) of the Cumulative Distribution Function (CDF) of ζ. When the PDF of the output quantity ζ is non-symmetric, a numerical value of α different from $(1 - p)/2$ may be more appropriate and it is given by the numerical value that minimizes the function $\Gamma_\zeta(\alpha) = G_\zeta^{-1}(p + \alpha) - G_\zeta^{-1}(\alpha)$. The values of $G_\zeta^{-1}(p + \alpha)$ and $G_\zeta^{-1}(\alpha)$ were computed as $(p + \alpha)$-quantile and α-quantile of G_ζ respectively for values of α in the range $[0, 1 - p]$ using the Matlab© function *prctile* [41]. The value of α that provided the minimum of the function $\Gamma_\zeta(\alpha)$ was then selected for the computation of the uncertainty interval.

V. Experimental Results

Nine dynamic tests were carried out to prove the repeatability of the results. In all the 9 tests, the acquisition frequency was set to $25\ kHz$ and the total acquisition time was at least $10\ s$. The experimental results are first shown in Fig. 6 and Fig. 7 and summarized in Table II. Specifically, Fig. 6 shows the fitting curve and the residuals of the nonlinear fitting of test 7 related to Method 3 applied to the peaks of the signal $x_l\ (t)$. The results for Method 3 obtained with the valleys are similar to the ones obtained with the peaks and are shown only in Table II for the sake of brevity. It can be observed that the residuals are

concentrated around zero, meaning that the 1 DOF 2nd-order underdamped mass-spring-damper model is a representative model of the longitudinal dynamics of the tape tether.
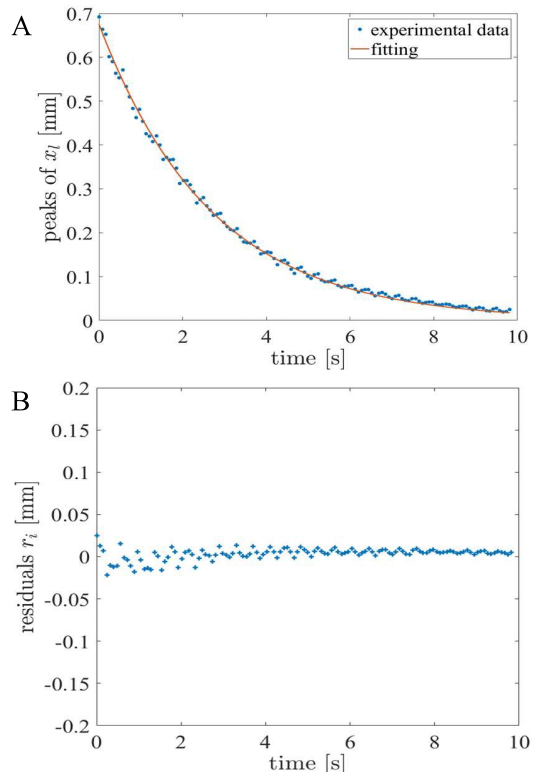
Fig. 6. Curve fitting (panel A) and residual (panel B) obtained with Method 3 (nonlinear fitting) applied to the peaks of the experimental data for test 7. The fitting curve is drawn in solid red line and the peaks are marked with blue dots.

The mean value of ζ over the 9 tests and for each method is shown in Fig. 7 and listed also in Table II, along with the associated extended uncertainty U_ζ. As is can be seen in Fig. 7, there is a band, the one marked with red dashed lines, that is common to the extended uncertainties of the 4 methods, meaning that the resulting values of ζ obtained with the 4 methods are in good agreement.

Fig. 8 shows the results of a MC analysis applied to test 1 with Method 4 to obtain the damping ratio distribution and compute the extended uncertainty $\tilde{U}_\zeta$. The frequency histogram is not symmetric and the procedure described in [40] was followed to properly compute $\tilde{U}_\zeta$, as described in the previous section. Fig. 9 shows the corresponding graph of the function $\Gamma_\zeta(\alpha)$ with the value of α that minimizes the function marked with a red dot.

The results of the MC analysis are shown for Method 1, Method 2, Method 3, and Method 4 in Fig. 10, Fig. 11, Fig. 12 and Fig. 13, respectively. In addition, Fig. 14 compares the uncertainty intervals obtained with the four methods analyzed in this work for the 9 tests. The employment of Method 1 leads to uncertainty intervals of ζ that are usually non-symmetric and larger than the other methods. In addition, we noticed that the frequency histogram of some tests, test 3 in particular, presents

---

[5] including the accuracy of the acquisition system.

This article has been accepted for publication in IEEE Transactions on Instrumentation and Measurement. This is the author's version which has not been fully edited and

7

a bi- or three- modal shape, revealing the presence of two or three distinct groups of individuals in the population. This means that Method 1 is more sensitive to the uncertainty sources than the other three methods. Concerning Methods 2 and 3, the uncertainty intervals of ζ obtained with peaks and those obtained with valleys are almost the same in all the 9 tests. In addition, the results of the MC analysis for the 9 tests are compatible, since the uncertainty intervals of the 9 tests share a common interval.

Concerning Method 4, the uncertainty intervals of ζ are shorter than those obtained with the other methods: this is because in Method 3 there are fewer uncertainty sources than in the other three methods. Moreover, the uncertainty sources for Method 4 that are associated with the initialization of the optimization algorithm (see Table I) involve parameters that the optimization algorithm computes to minimize the residuals. Those parameters converge to values that are poorly dispersed around their respective mean values, making ζ less sensitive to those uncertainty sources. In addition, Method 4 uses all the measurements acquired with the laser vibrometers and not just peaks or valleys as in the other three methods. On the other hand, the computational cost of Method 4 is higher than the other three methods since a minimization algorithm that employs all the acquired data is employed. Regarding the uncertainty intervals compatibility, there is a compatibility between tests from 2 to 8.

Referring to Fig. 14, there is a good compatibility between the uncertainty intervals of ζ obtained with Methods 2 and 4, except for test 1 only, and also between Methods 1 and 3.
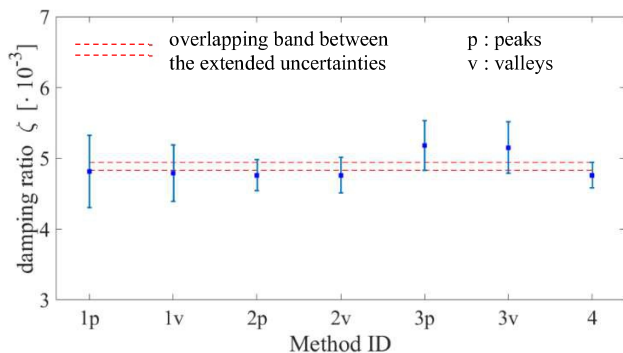
Fig. 7. Comparison between the mean values of the damping ratio ζ and associated extended uncertainties U_ζ (95% of confidence level) computed with the four methods analyzed in the paper (see also Table II).
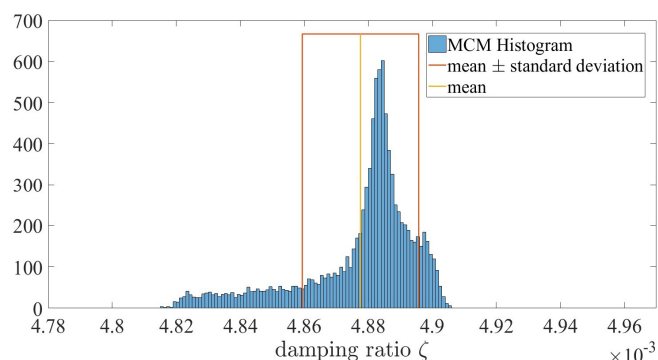

Fig. 8. Histogram showing the damping ratio ζ distribution obtained with a MC analysis applied to test 1 and for Method 4.
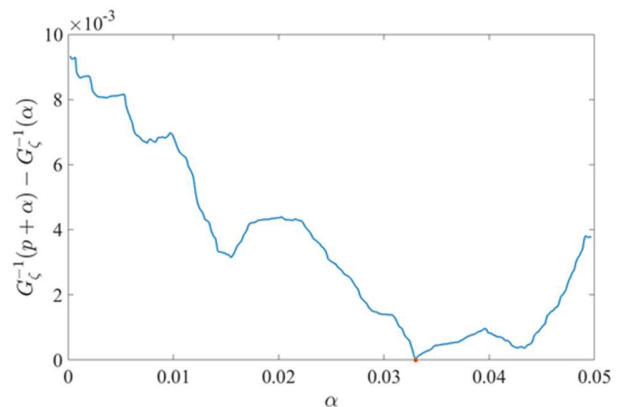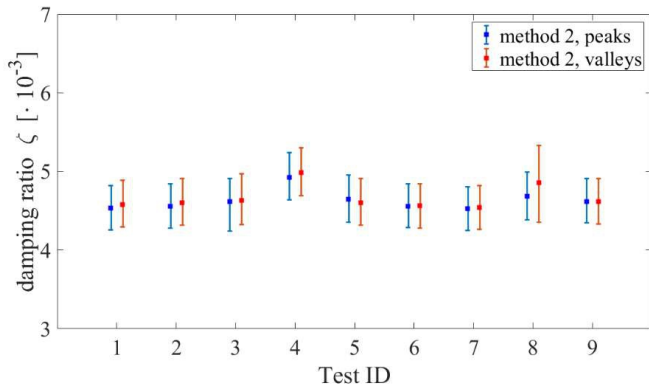

Fig. 9. Value of α computed as indicated in Supplement 1 of the ISO-GUM. The red dot represents the minimum of the function $\Gamma_\zeta(\alpha) = G_\zeta^{-1}(p + \alpha) - G_\zeta^{-1}(\alpha)$. This graph refers to Method 4 applied to test 1 and with $p = 0.95$.

TABLE II
MEAN VALUES OF THE DAMPING RATIO ζ AND
ASSOCIATED EXTENDED UNCERTAINTY U_ζ (95% OF
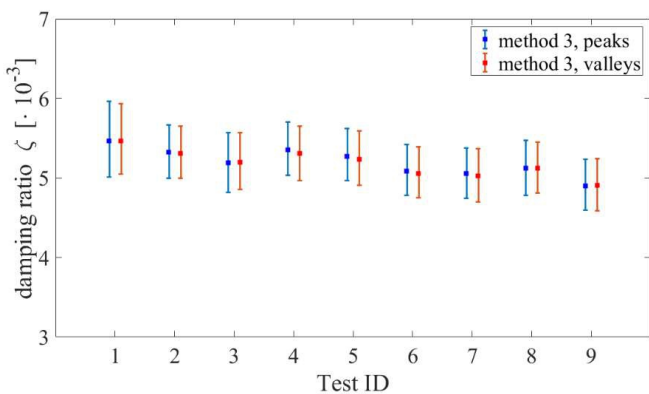CONFIDENCE LEVEL) FOR THE 4 METHODS
ANALYZED IN THIS PAPER

| Method	ID	damping ratio $\bar{\zeta}$ [$\cdot \mathbf{10^{-3}}$]	U_ζ (95%)
logarithmic decrement on peaks (p) and valleys (v)	1p	4.81	0.51
	1v	4.79	0.40
linear regression of peaks (p) and valleys (v) envelope	2p	4.76	0.22
	2v	4.76	0.25
nonlinear regression of peaks (p) and valleys (v) envelope	3p	5.18	0.35
	3v	5.15	0.36
nonlinear regression of filtered experimental data	4	4.76	0.18
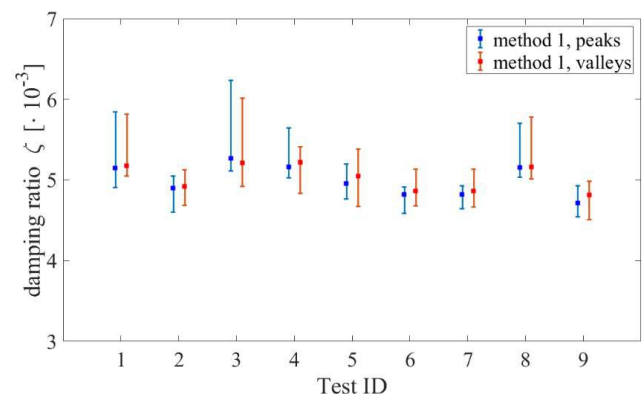
Fig. 10. Comparison between the mean values of the damping ratio ζ and associated extended uncertainties $\widetilde{U}_\zeta$ (95% of confidence level) computed with the MC analysis for Method 1 applied to peaks (blue) and valleys (red).

This article has been accepted for publication in IEEE Transactions on Instrumentation and Measurement. This is the author's version which has not been fully edited and
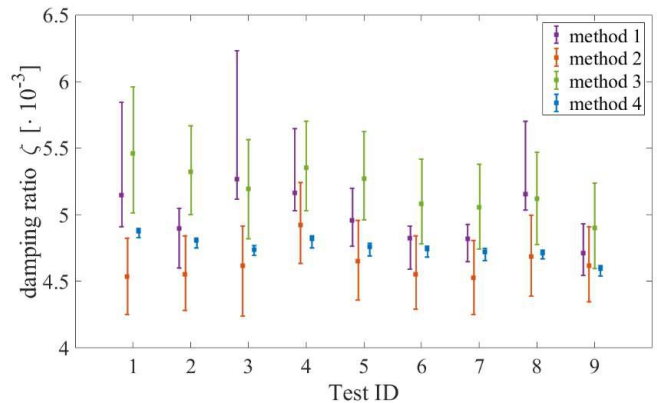
8

Fig. 11. Comparison between the mean values of the damping ratio ζ and associated extended uncertainties $\widetilde{U}_\zeta$ (95% of confidence level) computed with the MC analysis for Method 2 appalied to peaks (blue) and valleys (red).

Fig. 12. Comparison between the mean values of the damping ratio ζ and associated extended uncertainties $\widetilde{U}_\zeta$ (95% of confidence level) computed with the MC analysis for Method 3 appalied to peaks (blue) and valleys (red).
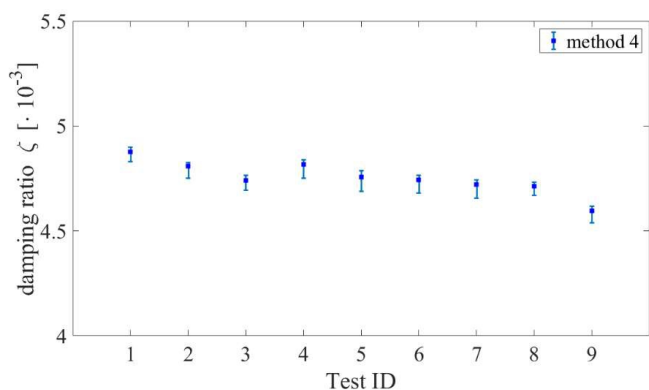
Fig. 13. Comparison between the mean values of the damping ratio ζ and associated extended uncertainties $\widetilde{U}_\zeta$ (95% of confidence level) computed with the MC analysis for Method 4.


Fig. 14. Comparison between the mean values of the damping ratio ζ and associated extended uncertainties $\widetilde{U}_\zeta$ (95% of confidence level) computed with the MC analysis for Method 1 appalied to peaks (violet), Method 2 applied to peaks (red), Method 3 applied to peaks (green) and Method 4 (blue).

Fig. 15 shows a comparison between the semi-amplitudes of the relative extended uncertainties (95% of confidence level) for the four methods. Method 4 provides a relative uncertainty interval which is less than ±1%, whereas for the other three methods the relative uncertainty interval is between ±6% and ±7%.
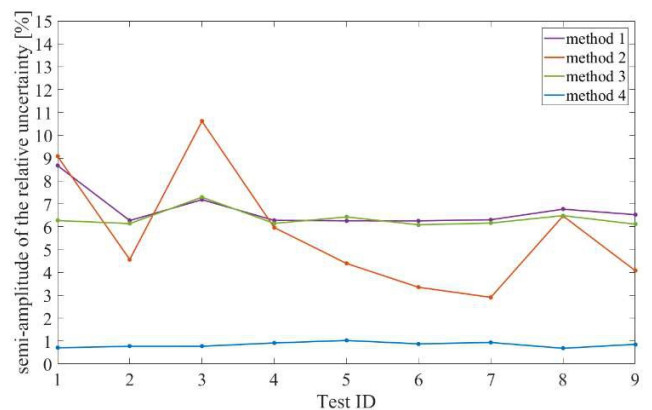
Fig. 15. Comparison between the semi-amplitude of the relative extended uncertainties (95% of confidence level) for the four methods analyzed in this paper.

The results of the damping ratio of a thin tape-shaped tether presented in this paper are valid for a temperature in the range 20 °C±1 °C where the experimental tests were conducted. Damping properties of materials are usually influenced by the temperature. As a future development, the proposed measurement apparatus could be adapted to operate in a thermal vacuum chamber, as the one used in [17], to characterize thin tapes for space applications in temperature ranges expected for specific mission scenarios.

VI. CONCLUSIONS

In this paper we presented a novel experimental setup and the methodology of analysis to measure precisely the damping ratio of thin tape-shaped tethers made of PEEK. A portion of this tape is used in the E.T.PACK project to provide dynamic

This article has been accepted for publication in IEEE Transactions on Instrumentation and Measurement. This is the author's version which has not been fully edited and

9

stability to the electrodynamic tether system during both deployment and deorbiting phases. A reliable and precise measurement of its mechanical characteristics including the damping ratio are important for evaluating their effects on the dynamic response and stability of a deorbiting system based on the green technology of electrodynamic tethers for mitigating the growth of orbital debris.

We used an experimental setup based on a laser vibrometer to measure without contact the longitudinal vibration of the tape tether made of PEEK. After applying a band-pass filter to the acquired signal to extract the vibrational mode of interest, we employed and compared four methods to analyze the filtered experimental data and estimate the damping ratio ζ. Specifically, the vibrational mode of interest is modelled as the response of a 2nd-order underdamped system to non-zero initial conditions and the four methods of analysis consist in applying: the classic logarithmic decrement method (Method 1); a linear regression (Method 2); a nonlinear regression (Method 3) on the extrema points of the filtered signal; and a nonlinear regression on all the acquired experimental data (Method 4).

In addition, following the ISO GUM, two kinds of extended uncertainty with an error risk of 5% were estimated. The first one is a repeatability uncertainty evaluated by repeating 9 times the experimental tests in the same operative conditions. Method 4 is the one that provides the smallest repeatability uncertainty: $\zeta = 4.76 \cdot 10^{-3} \pm 4\%$ with a confidence level of 95%. The second uncertainty type was estimated through a Monte Carlo analysis using 10000 trials and is due to the main uncertainty sources associated with the measurement system and the data analysis technique. A comparison between the resulting values of ζ computed with the four methods and with the associated extended uncertainties showed different widths of the uncertainty intervals. Although Method 4, that implements a nonlinear regression on all the acquired experimental data, has the highest computational cost, it shows a good consistency among the results of the 9 experimental tests and is the method that provides the smallest uncertainty interval, i.e., $\pm 1\%$ of the damping ratio estimation with a confidence level of 95%.

REFERENCES

[1] ESA Space Debris Office. "ESA's Annual Space Environment Report", ESA: Darmstadt, Germany, Rep. GEN-DB-LOG-00288-OPS-SD, 2020.

[2] Inter-Agency Space Debris Coordination Committee, "IADC Statement on Large Constellations of Satellites in Low Earth Orbit", Rep. IADC-15-03, July 2021.

[3] S. Hobbs, G. Stansbery, T. M. de Carvalho, "Space Waste", chapter 30, Waste, Second Edition, Academic Press, 2019, ch 30, pp. 567-583, ISBN 9780128150603. doi: https://doi.org/10.1016/B978-0-12-815060-3.00030-X.

[4] A. G. Karacalioglu and J. Stupl, "The Impact of New Trends in Satellite Launches on the Orbital Debris Environment", NASA, Houston, TX, United States, 2016.

[5] B. Virgili et al., "Risk to space sustainability from large constellations of satellites", Acta Astronautica, vol. 126, pp. 154-162, 2016, ISSN 0094-5765, doi: https://doi.org/10.1016/j.actaastro.2016.03.034.

[6] L. Olivieri and A. Francesconi. "Large constellations assessment and optimization in LEO space debris environment", Advances in Space Research, vol 65, no. 1, pp 351-363, 2020, ISSN 0273-1177, doi: https://doi.org/10.1016/j.asr.2019.09.048..

[7] S. Kawamoto, N. Nagaoka, T. Sato, and T. Hanad, "Impact on collision probability by post mission disposal and active debris removal", Journal of Space Safety Engineering, vol. 7, no. 3, pp. 178-191, 2020, ISSN 2468-8967, doi: https://doi.org/10.1016/j.jsse.2020.07.012.

[8] H. Stokes et al., "Evolution of ISO's space debris mitigation standards", Journal of Space Safety Engineering, vol. 7, no. 3, pp. 325–331, 2020, ISSN 2468-8967, doi: https://doi.org/10.1016/j.jsse.2020.07.004.

[9] P. Tadini et al., "Active debris multi-removal mission concept based on hybrid propulsion", Acta Astronautica, vol. 103, pp. 26-35, 2014, ISSN 0094-5765, https://doi.org/10.1016/j.actaastro.2014.06.027.

[10] Office For Outer Space Affairs, "Space Debris Mitigation Guidelines of the Committee on the Peaceful Uses of Outer Space", United Nations, Vienna, 2010.

[11] Inter-Agency Space Debris Coordination Committee, "IADC Space Debris Mitigation Guidelines", IADC, Rep. IADC-02-01, Rev. 2, March 2020.

[12] L. Anselmo and C. Pardini, "Compliance of the Italian satellites in low Earth orbit with the end-of-life disposal guidelines for Space Debris Mitigation and ranking of their long-term criticality for the environment", Acta Astronautica, vol. 114, pp. 93-100, 2015, ISSN 0094-5765, doi: https://doi.org/10.1016/j.actaastro.2015.04.024.

[13] C. Colombo et al., "Effects of passive de-orbiting through drag and solar sails and electrodynamic tethers on the space debris environment", in Proc. 69th IAC, Bremen, Germany, 2018.

[14] A. Rossi et al., "ReDSHIFT: A Global Approach to Space Debris Mitigation," Aerospace, vol. 5, no. 2, p. 64, Jun. 2018, doi: 10.3390/aerospace5020064.

[15] G. Sarego et al., "Impact risk assessment of deorbiting strategies in Low Earth Orbits", in Proc. ASCEND 2021, Las Vegas, Nevada & Virtual, 2021.

[16] G. Sanchez-Arriaga and X. Chen, "Modeling and performance of electrodynamic low-work-function tethers with photoemission effects", Journal of Propulsion and Power, vol. 34, no. 1, pp. 213–220, 2018, doi: 10.2514/1.B36561.

[17] I. C. Bell, B. E. Gilchrist and J. K. McTernan, "Analyzing Miniature Electrodynamic Tether Propulsion Capabilities and the Interaction with the Low Earth Orbit – Plasma Environment", in Proc. Spacecraft Charging Technology Conference, 2014.

[18] T. Sato et al., "A Study on PMD Device for Microsatellites Using Electrodynamic Tether", Trans. JSASS Aerospace Tech., vol. 19, no. 1, pp. 61-67, 2021, doi: 10.2322/tastj.19.61.

[19] J.R. Sanmartin, M. Martinez-Sanchez, E. Ahedo, "Bare wire anodes for electrodynamic tethers", J. Propulsion and Power 9, (1993) 353–360, doi: 10.2514/3.23629.

[20] M. L. Cosmo and E. C. Lorenzini, "Tethers In Space Handbook", December 1, 1997. [Online] Available: https://ntrs.nasa.gov/citations/19980018321.

[21] A. Francesconi, C. Giacomuzzo, F. Branz and E. C. Lorenzini "Survivability to hypervelocity impacts of electrodynamic tape tethers for deorbiting spacecraft in LEO", in Proc. 6th European conference on space debris, Darmstadt, Germany, April 2013.

[22] K. Makihara and S. Kondo, "Structural Evaluation for Electrodynamic Tape TethersAgainst Hypervelocity Space Debris Impacts", AIAA Journal of Spacecraft and Rockets, vol. 55, no. 2, 2018, pp. 462-472, doi: 10.2514/1.A34023.

[23] S. B. Khan et al., "Survivability to orbital debris of tape tethers for end-of-life spacecraft de-orbiting", Aerospace Science and Technology, vol. 52, pp. 167-172, 2016, ISSN 1270-9638, doi: 10.1016/j.ast.2016.02.033.

[24] G. Sarego et al., "Deployment requirements for deorbiting electrodynamic tether technology", CEAS Space Journal, vol. 13, no. 4, pp. 567 − 581, 2021, doi: 10.1007/s12567-021-00349-5.

[25] R. Mantellato, M. Pertil, G. Colombatti, A. Valmorbida and E. C. Lorenzini, "Two-bar model for free vibrations damping of space tethers by means of spring-dashpot devices", CEAS Space Journal, vol. 6, no. 3, pp. 133 - 143, 2014, doi: 10.1007/s12567-014-0065-x.

[26] E. M. Silverman and R. Griese, "Property performance of thermoplastic composites for spacecraft systems", *SAMPE J.*, vol. 25, no. 6, pp. 38-47, 1989.

[27] L. Tarabini Castellani *et al.*, "Deorbit kit demonstration mission", *Journal of Space Safety Engineering*, vol. 9, no. 2, pp. 165-173, 2022, ISSN 2468-8967 , doi: 10.1016/j.jsse.2022.01.004.

[28] A. Valmorbida, L. Olivieri, A. Brunello, G. Sarego, G. Sánchez-Arriaga, E.C. Lorenzini, "Validation of enabling technologies for deorbiting devices based on electrodynamic tethers." *Acta Astronautica*, vol. 198, pp. 707-719, 2022, ISSN 0094-5765, doi: 10.1016/j.actaastro.2022.06.013.

[29] J. Vanwalleghem *et al.*, "Practical aspects in measuring vibration damping of materials", in *Proc. 15th International Conference on Experimental Mechanics*, Porto, Portugal, July 2012.

[30] K. Kunugi, H. Kojima and P. M. Trivailo, "Modeling of tape tether vibration and vibration sensing using smart film sensors", *Acta Astronautica*, vol. 107, pp. 97-111, 2015, ISSN 0094-5765, doi: 10.1016/j.actaastro.2014.11.024.

[31] M. S. Allen and M. W. Sracic, "A new method for processing impact excited continuous-scan laser Doppler vibrometer measurements", *Mechanical Systems and Signal Processing*, vol. 24, no. 3, pp. 721-735, 2010, ISSN 0888-3270, doi: 10.1016/j.ymssp.2009.11.004.

[32] R. Pereira, J. P. Arenas and E. Zumelzu, "Comparison of four test methods to measure damping properties of materials by using piezoelectric transducers", *Materials & Design*, vol. 32, no. 4, pp. 2423-2428, 2011, ISSN 0261-3069, doi: 10.1016/j.matdes.2010.11.070.

[33] A. Valmorbida, M. Mazzucato, S. Tronco, S. Debei and E. C. Lorenzini, "SPARTANS - A cooperating spacecraft testbed for autonomous proximity operations experiments", in *Proc. 2015 IEEE International Instrumentation and Measurement Technology Conference (I2MTC)*, 2015, pp. 739-744, doi: 10.1109/I2MTC.2015.7151360.

[34] A. Brunello, L. Olivieri, G. Sarego, A. Valmorbida, E. Lungavia and E. C. Lorenzini, "Space tethers: parameters reconstructions and tests", in *Proc. 2021 IEEE 8th International Workshop on Metrology for AeroSpace (MetroAeroSpace)*, 2021, pp. 235-240, ISSN: 2575-7490, doi: 10.1109/MetroAeroSpace51421.2021.9511677.

[35] A. Valmorbida *et. al*, "Measurement of mechanical characteristics of tape tethers for space applications", in *Proc. 2022 IEEE 9th International Workshop on Metrology for AeroSpace (MetroAeroSpace)*, Pisa, Italy, 2022, pp. 293-298, doi: 10.1109/MetroAeroSpace54187.2022.9856266.

[36] H. Yamakawa, H. Hosaka, H. Osumi and K. Itao, "Development of a system for measuring structural damping coefficients", *Human Friendly Mechatronics*, selected papers of the ICMA2000, pp. 259-264, 2001, ISBN 9780444506498, doi: 10.1016/B978-044450649-8/50044-9.

[37] D. D. Milašinović, "Rheological–dynamical analogy: Prediction of damping parameters of hysteresis damper", *International Journal of Solids and Structures*, vol. 44, no. 22–23, pp. 7143-7166, 2007, ISSN 0020-7683, doi: 10.1016/j.ijsolstr.2007.04.001.

[38] C. M. Harris, C. E. Crede, Shock and vibration handbook, McGraw-Hill, New York , 1976.

[39] BIPM, IEC, IFCC, ILAC, ISO, IUPAC, IUPAP, OIML, "Evaluation of Measurement Data – Guide to the Expression of Uncertainty in Measurement", International Organization for Standardization, Geneva, Switzerland, 2008.

[40] BIPM, IEC, IFCC, ILAC, ISO, IUPAC, IUPAP, OIML, "Evaluation of measurement data – Supplement 1 to the Guide to the expression of uncertainty in measurement – Propagation of distributions using a Monte Carlo method", International Organization for Standardization, Geneva, Switzerland, 2008.

[41] E. Langford, "Quartiles in Elementary Statistics", *Journal of Statistics Education*, vol. 14, no. 3, 2006, doi: 10.1080/10691898.2006.11910589.